Journal of Applied Physics ARTICLE scitation.org/journal/jap

Role of phonon coupling and non-equilibrium near the interface to interfacial thermal resistance: The multi-temperature model and thermal circuit

Cite as: J. Appl. Phys. **125**, 085107 (2019); doi: 10.1063/1.5082526
Submitted: 21 November 2018 · Accepted: 17 February 2019 ·
Published Online: 28 February 2019

Zexi Lu, Jingjing Shi, and Xiulin Ruan

AFFILIATIONS

School of Mechanical Engineering, Purdue University, West Lafayette, Indiana 47907, USA

ABSTRACT

Interfacial thermal transport between two semi-infinite leads has been widely assumed to be independent from bulk transport in the two leads. However, here we show that due to the mismatch of phonon modal interfacial conductance and modal thermal conductivity, thermal interfacial transport is affected by the bulk thermal transport, and phonons near the interface can be driven into strong non-equilibrium, causing an additional resistance that is lumped into the interfacial resistance. This is captured using a multi-temperature model (MTM) that we introduce. Using thermal properties predicted from first-principles calculations and interfacial transmission coefficients predicted from the acoustic mismatch model, we present a case study of thermal transport across the Si-Ge interfaces using our MTM. The results show that phonon branches are in non-equilibrium near the interface due to energy re-distribution caused by different thermal properties of the materials and the corresponding transmission coefficients, and the overall interfacial thermal conductance is 5.4% smaller than the conventional prediction, due to the phonon non-equilibrium resistance. We present a thermal circuit to include this new resistance due to phonon-phonon coupling and non-equilibrium near the interfaces. The thermal circuit also shows that increasing the phonon-phonon coupling factor G_{pp} can reduce this resistance. Our MTM is a general and simple analytical approach expected to be useful for investigating the coupling between thermal transport across interfaces and in the bulk leads.

I. INTRODUCTION

Nowadays, as electronic devices shrink into nano-scale, interfacial heat generation and dissipation become critical issues in designing these nano-structures. The prediction and measurement of interfacial thermal conductance (ITC) between different materials have been drawing attention among the research community. Traditional prediction methods for the lattice portion of ITC include calculations based on the acoustic mismatch model (AMM), diffuse mismatch model (DMM), atomistic Green's function, molecular dynamics (MD), and density functional theory.[1–4] Among them, DMM is often used to provide a reference for experimental measurements due to its practical simplicity and its advantage in describing the interface between dissimilar materials. The lattice ITC is then calculated using the Landauer approach as follows:

$$h = \int_0^\infty D(\omega)\tau(\omega)v_g\hbar\omega\frac{df_{BE}}{dT}d\omega. \quad (1)$$

Here, ω is the phonon frequency, D is the density of states, τ is the transmission, f_{BE} is the Bose-Einstein distribution function, and T is the temperature. Using Eq. (1), three important assumptions are made: (1) elastic phonon scattering, which means that the number of phonons is conserved. Phonons are either reflected or transmitted at the interface without changes in the frequency. (2) Local thermal equilibrium, where the measurable temperature of all phonon modes at the interface, is their common emitting temperature. This also leads to an important outcome that (3) the interfacial thermal transport is assumed to be completely decoupled from the bulk transport in the two semi-infinite leads. However, recently both experimental and theoretical studies have cast serious questions to these three assumptions. Regarding the first assumption, measurements of ITC at several metal-diamond interfaces exceed the upper limits of Landauer predictions by 20% to as large as 10 times,[5–7] as well as simulations and calculations demonstrating the inelastic phonon scattering induced by anharmonicity in the lattice, which facilitates the interfacial transport.[8–15] Regarding the second assumption, it has been demonstrated that during many applications such as irradiation-matter interactions, phonons can be driven into strong non-equilibrium by mechanisms such as selective

electron-phonon (*e-p*) coupling, and a simple equilibrium picture leads to misleading or wrong results. For example, in Raman spectroscopy measurement of graphene's thermal conductivity, a simple two-temperature model (TTM) assuming local thermal equilibrium will under-predict the thermal conductivity by more than 50%.[16,17] Strong phonon local non-equilibrium has also been observed at the interfaces in MD simulations.[10,18,19] Similarly, the *e-p* non-equilibrium at metal-dielectric interfaces has been proved to contribute to the interfacial thermal resistance.[20–24] These observations motivated a recent study of Shi *et al.*, where it was pointed out that the measurable temperatures of phonon modes at the interface are not their emitting temperatures but equivalent equilibrium temperatures.[25] They proposed a non-equilibrium Landauer approach that can increase the ITC significantly as compared to the original one. However, the work focused on the interface itself and did not consider any possible coupling between interfacial and bulk transports yet. The observation of *e-p* non-equilibrium across the metal-nonmetal interfaces[26–28] inspired us to hypothesize that similar local non-equilibrium could exist among different phonon modes or branches near the interface, and add additional contribution to the interfacial resistance. A method that can capture this non-equilibrium feature and quantitatively predict its impact is necessary.

In this study, we will present a multi-temperature model (MTM) simulation approach which can capture the coupling between interfacial and bulk thermal transports and the resulting phonon non-equilibrium thermal transport process. Here, we only consider elastic phonon transmission in the model, but the framework allows for adding inelastic scattering. Phonon scattering is described by defining an averaged scattering lattice reservoir with which all phonon branches couple, and the coupling strengths are determined using the relaxation time approximation (RTA). The phonon branch-resolved ITCs are calculated using AMM applied to each phonon branch.

II. THEORY AND GOVERNING EQUATIONS

We choose the Si-Ge interfaces to investigate the coupling between bulk and interfacial transport since both materials have six phonon branches [1 longitudinal acoustic (LA) branch, 2 transverse acoustic (TA) branches, 1 longitudinal optical (LO) branch, and 2 transverse optical (TO) branches], and the thermal properties have been well predicted in previous literature.[29] The system consists of a 500 nm-long Si block in contact with a 500 nm-long Ge block, as is shown in Fig. 1. The length of the system is much larger than the phonon mean free path in the two materials so that the diffusive transport can be assumed. In order to investigate the coupled thermal transport, a method that can resolve the temperatures of different phonon modes and capture the coupling among them is needed. The MTM with *e-p* coupling has been introduced in our previous works.[16,30] In this work, we aim at predicting the effect of non-equilibrium thermal transport on lattice ITC, and therefore we only focus on the lattice portion. The governing equation is

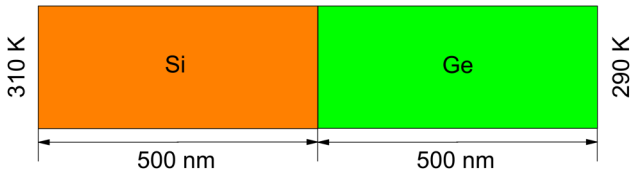

FIG. 1. Illustration of the simulation domain.

$$C_{p,i}\frac{\partial T_{p,i}}{\partial t} = k_{p,i}\frac{\partial^2 T_{p,i}}{\partial x^2} + G_{pp,i}(T_{lat} - T_{p,i}), \tag{2}$$

where i is the index of phonon branches. Equation (2) describes the multi-channel coupled energy transfer process in dielectrics. Here, t is the time, k and C refer to the thermal conductivity and volumetric heat capacity of the energy carriers, respectively, i is the index for phonon branches, $G_{pp,i}$ is the phonon-phonon (*p-p*) coupling factor between phonon branch i and the "scattering lattice reservoir" that is represented by an averaged T_{lat}. $G_{pp,i}$ is calculated using RTA from the following equation:[31,32]

$$G_{pp,i} = \frac{C_{p,i}}{\tau_i}, \tag{3}$$

where τ_i is the relaxation time of phonon branch i. The phonon scattering is then described by the last term in Eq. (2). It is an analogy of the *e-p* coupling in TTM using RTA based on the assumption that the *p-p* scattering has negligible effects on phonon distribution and phase space. T_{lat} is defined to ensure that the energy transfer among phonon branches is conserved

$$\sum G_{pp,i}(T_{lat} - T_{p,i}) = 0. \tag{4}$$

The input thermal properties are listed in Table I. At the interface, the boundary condition for each phonon branch is described using the Neumann boundary condition

$$J_i = h_i(T_{1,i} - T_{2,i}), \tag{5}$$

where $T_{1,i}$ and $T_{2,i}$ are the temperatures at the two interfaces.[33] The phonon branch-resolved ITCs in Eq. (5) are predicted using AMM. The transmission function of a single phonon mode with frequency ω for the interface between 3D materials from AMM is shown in the following equation:[1]

$$t_{12}(\theta_1, \omega) = t_{21}(\theta_2, \omega) = \frac{4\frac{Z_2\cos\theta_2}{Z_1\cos\theta_1}}{\left(\frac{Z_2}{Z_1} + \frac{\cos\theta_2}{\cos\theta_1}\right)^2}, \tag{6}$$

where θ_1 is the angle of incidence, θ_2 is the angle of refraction, and Z is the acoustic impedance which equals the product of the material mass density ρ and the phonon group velocity v_g. With the transmission coefficient from AMM, the heat flux J_i of phonon branch i (unit: W/m^2) and "dressed" ITC h_i can be calculated from the Landauer approach[25]

$$J_i = \frac{1}{2}\int_0^{\frac{\pi}{2}}\int_0^{+\infty} \hbar\omega_i[D_1(\omega_i)v_{g1,i}(\omega_i)t_{12,i}(\theta_{1,i}, \omega_i)f_{BE}(T_{e1,i})\sin\theta_i\cos\theta_i] \times d\omega_i d\theta_i - \frac{1}{2}\int_0^{\frac{\pi}{2}}\int_0^{+\infty} \hbar\omega_i[D_2(\omega_i)v_{g2,i}(\omega_i)t_{21,i}(\theta_{2,i}, \omega_i) \times f_{BE}(T_{e2,i})\sin\theta_i\cos\theta_i]d\omega_i d\theta_i,$$

TABLE I. Input thermal properties of Si and Ge at 297 K. The properties are taken from Ref. 29, while the $G_{pp,i}$'s are calculated using Eq. (3) and h's are calculated as the "dressed" conductance according to Ref. 25. The values for TA or TO phonons represent a single TA or TO branch. Units for the values are as follows: $G_{pp}(10^{16}\,\mathrm{W/m^3\,K})$, $C_p(10^5\,\mathrm{J/m^3\,K})$, τ(ps), k(W/m K), and $h(\mathrm{MW/m^2\,K})$.

	Si					Interface		Ge				
	$G_{pp,i}$	$C_{p,i}$	τ_i	k_i	k_i%	h_i	h_i%	$G_{pp,i}$	$C_{p,i}$	τ_i	k_i	k_i%
LA	0.8	1.8	21.7	53.6	34.7	243.8	61.4%	0.5	1.6	30.1	20.2	56.6
TA	0.2	2.0	136.4	49.1	31.8	76.4	19.3%	0.1	1.6	188.4	7.1	19.9
LO	3.7	1.4	3.8	2.5	1.6	0	0	3.1	1.5	4.8	1.1	3.1
TO	4.1	1.2	3.0	0.1	0.1	0	0	3.6	1.4	4.0	0.1	0.5

$$h_i = \frac{J_i}{\Delta T_i} = \frac{J_i}{(T_{1,i} - T_{2,i})}. \tag{7}$$

Here, $T_{e1,i}$ and $T_{e1,i}$ are the emitting temperatures of the phonons at the two interfaces.[33] Our calculation assumes that the interfacial transmission does not change the phonons' vibration patterns, so Eqs. (6) and (7) are applied to each phonon branch. The results are listed in Table I. Because the optical phonon branches have no frequency overlaps, their h's are all 0.

III. RESULTS AND DISCUSSIONS

Calculations are performed using the discretized form of Eq. (2). The two ends of the system are fixed at 310 K and 290 K, respectively, and heat flows in the direction perpendicular to the interface. Initially, the entire system is at 300 K and then the simulation runs for 50 ns to ensure steady state are reached. The steady-state temperature profile is shown in the upper part of Fig. 2. It can be seen that the degree of non-equilibrium is not very strong at such interfaces. Different phonon branches are in equilibrium in most parts of the Ge block. The cooling length, defined as the distance for the largest temperature deviation between phonon branches to reach $1/e^3$ of its maximum value, is smaller than 50 nm in Ge. The non-equilibrium is stronger in Si with a cooling length of approximately 200 nm, but the temperature deviation is small compared to the temperature jump across the interface. The optical phonon branches have almost identical temperatures with T_{lat} due to their large G_{pp} values, while the non-equilibrium is stronger among acoustic branches.

A. Coupling between bulk and interfacial transports

The phonons' relative contributions to the thermal transport are plotted in the lower part of Fig. 2. Away from the interface, each phonon branch has a constant heat flux determined by its thermal conductivity. As the position approaches the interface, the TA phonons get a higher temperature than T_{lat} and dump energy to the lattice reservoir, resulting in a decreased heat flux near the interface, while the LA phonons have a lower temperature and receive energy leading to an increased heat flux. This process of energy re-distribution can be directly explained by the k_i% and h_i% values in Table I, which represent the ratio of k_i and h_i of each phonon branch i over the total value, respectively. In Si, the k_i%

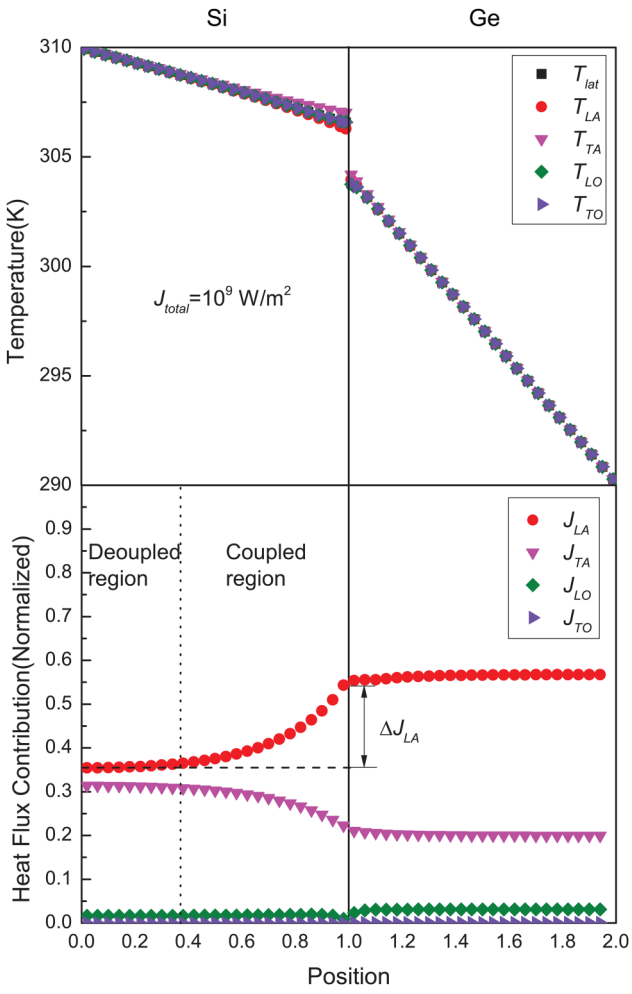

FIG. 2. The steady-state temperature profile and contribution of each phonon branch to the thermal transport of a Si-Ge interface. The degree of non-equilibrium induced by p-p coupling is not very strong, with all phonon branches in thermal equilibrium in most parts of the system. The position is normalized by the length of each block, and heat fluxes are normalized by their total value. The coupled and decoupled regions are only shown in the Si block.

values are similar for LA and TA phonons indicating that they contribute similarly, while in Ge, the LA phonons contribute a lot more than the TA phonons. When heat goes from Si to Ge, the energy has to re-distribute gradually from the Si ratio to the Ge. As they move in Si towards the interface, LA phonons gradually receive energy resulting in an increased heat flux, and their transmission to Ge is ensured by their larger ITC. TA phonons, on the contrary, lose heat and only needs a smaller ITC across the interface. Similar to the concept of cooling length, we can define the "coupled" and "decoupled" regions for thermal transport. Taking the change in heat flux ΔJ as the standard, as shown in Fig. 2 using the LA phonons as an example, we define the region over which ΔJ diminishes to $1/e^3$ of its maximum value as the coupled region and the rest as the decoupled region. Then, it is straightforward to see that in the decoupled region, the thermal transport is determined by the bulk properties of the material and independent of the interfacial conditions. The coupled region is where phonons go through the energy re-distribution process. The relative contributions of different phonons are significantly affected by the local non-equilibrium due to the interfacial transmission coefficient, resulting in the coupled thermal transport between bulk and interface. The size of the coupled regions is determined by both materials, and for a Si-Ge interface it is 320 nm in Si and 10 nm in Ge. It is noteworthy that although in Fig. 2 we show ΔJ_{LA} as an example to define the coupled region, the result is the same regardless of which phonon branch one chooses.

B. The interfacial conductance

The total ITC across the interface is calculated by extrapolating the linear equilibrium section of the temperature profile to the interface to obtain the averaged temperature jump ΔT_{fit}, as shown in Fig. 3. Note that T_{fit} is different from T_{lat}; therefore the lattice temperature should not be used directly for calculating ITC at interfaces with thermal non-equilibrium. The result of $h_{MTM} = J_{total}/\Delta T_{fit}$ is 375.1 MW/m^2 K. Compared with the classical ITC based on the local thermal equilibrium assumption, which is acquired by summing up the branch-resolved AMM results $h_{LA} + 2h_{TA} = 396.6$ MW/m^2 K as can be easily verified using Eqs. (6) and (7), h_{MTM} is 5.4% smaller. This can be explained by the non-equilibrium in phonon temperatures. For LA and TA phonons, the ITCs calculated from AMM satisfy the following equations:

$$\begin{aligned} h_{LA} &= \tfrac{J_{LA}}{\Delta T_{LA}}, \\ h_{TA} &= \tfrac{J_{TA}}{\Delta T_{TA}}. \end{aligned} \tag{8}$$

When we use T_{fit} to calculate the ITC, ΔT_{LA} is over-predicted ($\Delta T_{fit} > \Delta T_{LA}$), resulting in an under-prediction of LA phonons' contribution to the total ITC. The TA phonons, on the other hand ($\Delta T_{fit} < \Delta T_{TA}$), can be directly verified to be over-predicted. The competing effect between TA and LA eventually results in the following relation:

$$\begin{aligned} h_{MTM} &= \frac{J_{total}}{\Delta T_{fit}} = \frac{J_{LA}}{\Delta T_{fit}} + 2\frac{J_{TA}}{\Delta T_{fit}} < \frac{J_{LA}}{\Delta T_{LA}} + 2\frac{J_{TA}}{\Delta T_{TA}} \\ &= h_{LA} + 2h_{TA}, \end{aligned} \tag{9}$$

since LA phonons are the major contributor to the thermal transport. It is straightforward to verify that if all phonons are in thermal equilibrium, h_{MTM} should be identical to $h_{LA} + 2h_{TA}$. Therefore, it is reasonable to conclude that this discrepancy originates from the non-equilibrium phonon thermal transport at the interface, and it is similar with the *e-p* non-equilibrium that occurs at the metal-dielectric interfaces, which also introduces additional interfacial thermal resistance.

Now, we can construct a thermal circuit using our results and those from works considering inelastic transmission.[8–15] Inelastic

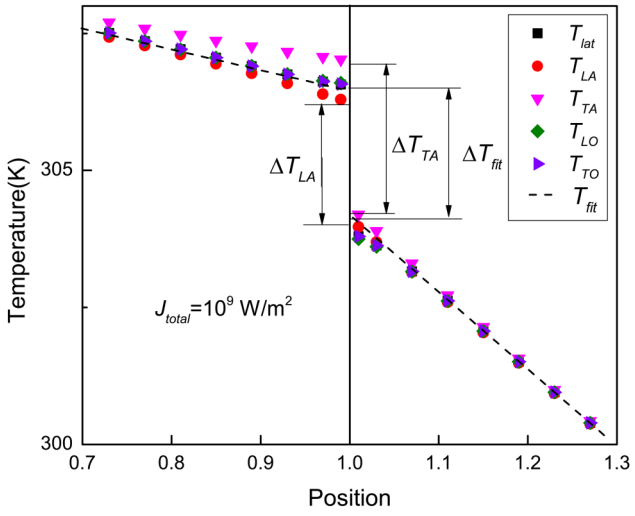

FIG. 3. A zoomed-in picture of the temperature profile of the Si-Ge interface. The fitted temperature T_{fit} is acquired by extrapolating the linear equilibrium part of the temperature profile. It can be observed that $\Delta T_{fit} > \Delta T_{LA}$ and $\Delta T_{fit} < \Delta T_{TA}$.

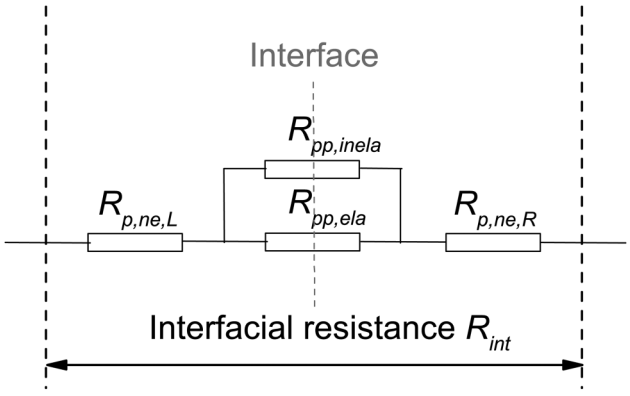

FIG. 4. A thermal circuit representing the conduction near the interface when including the thermal non-equilibrium and inelastic scattering physics. The inelastic scattering forms an additional interfacial energy transfer channel $R_{pp,inela}$ that is in parallel with the classical elastic scattering channel $R_{pp,ela}$, while the non-equilibrium acts as resistances $R_{p,ne}$'s in series with the two and hinders heat transfer. The subscripts *L* and *R* denote the materials in the left and right, respectively, which in our case study are Si and Ge.

TABLE II. Thermal resistances at the interface.

$R_{p,ne} = R_{p,ne,L} + R_{p,ne,R} = 0.145 \times 10^{-9}\ \mathrm{m^2\,K/W}$	$R_{pp,ela} = 2.521 \times 10^{-9}\ \mathrm{m^2\,K/W}$
$R_{int} = R_{p,ne} + R_{pp,ela} = 2.666 \times 10^{-9}\ \mathrm{m^2\,K/W}$	

phonon transmission, induced by lattice anharmonicity, allows phonons to change their frequency when transferring across the interface. Compared with the conventional elastic scattering channel $R_{pp,ela}$ which is considered by AMM, DMM, Landauer equation, and our approach, inelastic transmission adds an additional energy transfer channel $R_{pp,inela}$ as shown in Fig. 4. The *p-p* non-equilibrium resistances $R_{p,ne}$'s are in series with the phonon transmission resistance while not in parallel with them. This is in analogy to the *e-p* non-equilibrium resistance in the thermal circuit for the metal-nonmetal interfaces (Refs. 20–22 and 24). From our simulation, we can derive the values of the resistances in this network, as listed in Table II. Because inelastic transmission is not considered in our work, only $R_{p,ne}$ and $R_{pp,ela}$ are listed. $R_{pp,ela}$ and R_{int} are acquired by taking the inverse of $h_{LA} + 2h_{TA}$ and h_{MTM}, respectively. It can be noted that although increasing *p-p* anharmonic coupling G_{pp} will decrease the thermal conductivity, it increases ITC by decreasing both $R_{p,ne}$ and $R_{pp,inela}$. This thermal circuit gives good insights into previous MD simulations where larger anharmonicity was observed to enhance ITC.[10]

IV. SUMMARY

We have presented the coupling between bulk and interfacial transport in the Si-Ge interfaces, based on our multi-temperature simulation approach that can predict phonon branch-resolved temperature profile and capture the non-equilibrium thermal transport process. Local thermal non-equilibrium between different phonon branches is observed due to an energy re-distribution process phonons go through, which is determined by their different *k*% values in different materials and the corresponding transmission coefficients at the interface. The results show that the ITC from the simulation is 5.4% smaller than the classical prediction based on the local thermal equilibrium assumption, and the discrepancy originates from the phonon thermal non-equilibrium near the interface. The impact of non-equilibrium phonon thermal transport on ITC is not very significant at the Si-Ge interfaces and therefore may not readily answer the unresolved questions. Our MTM is still a general approach and can be applied to materials where non-equilibrium is stronger than Si-Ge and better manifest the coupled thermal transport. It is also an important task for experimentalists to directly probe such local non-equilibrium near the interfaces. Our framework can also include inelastic phonon transmission in the future.

ACKNOWLEDGMENTS

The authors thank the support from the Defense Advanced Research Projects Agency (Award No. HR0011-15-2-0037).

REFERENCES

[1]E. T. Swartz and R. O. Pohl, Rev. Mod. Phys. **61**, 605 (1989).
[2]J. T. Gaskins, G. Kotsonis, A. Giri, C. T. Shelton, E. Sachet, Z. Cheng, B. M. Foley, Z. Liu, S. Ju, Junichiro, M. S. Goorsky, S. Graham, T. Luo, A. Henry, J.-P. Maria, and P. E. Hopkins, Nano Lett. **18**(12), 7469–7477 (2018).
[3]E. S. Landry and A. J. H. McGaughey, J. Appl. Phys. **107**, 013521 (2010).
[4]S. Baroni, S. de Gironcoli, A. Dal Corso, and P. Giannozzi, Rev. Mod. Phys. **73**, 515 (2001).
[5]R. J. Stoner and H. J. Maris, Phys. Rev. B **48**, 16373 (1993).
[6]H.-K. Lyeo and D. G. Cahill, Phys. Rev. B **73**, 144301 (2006).
[7]G. T. Hohensee, R. B. Wilson, and D. G. Cahill, Nat. Commun. **6**, 6578 (2015).
[8]P. E. Hopkins, J. Appl. Phys. **106**, 013528 (2009).
[9]P. E. Hopkins and P. M. Norris, J. Heat Transfer **131**, 022402 (2009).
[10]X. Wu and T. Luo, J. Appl. Phys. **115**, 014901 (2014).
[11]K. Gordiz and A. Henry, Sci. Rep. **6**, 23139 (2016).
[12]N. Q. Le, C. A. Polanco, R. Rastgarkafshgarkolaei, J. Zhang, A. W. Ghosh, and P. M. Norris, Phys. Rev. B **95**, 245417 (2017).
[13]Y. Zhou and M. Hu, Phys. Rev. B **95**, 115313 (2017).
[14]E. Lee and T. Luo, Appl. Phys. Lett. **112**, 011603 (2018).
[15]T. Feng, Y. Zhong, J. Shi, and X. Ruan, Phys. Rev. B **99**, 045301 (2019).
[16]A. K. Vallabhaneni, D. Singh, H. Bao, J. Murthy, and X. Ruan, Phys. Rev. B **93**, 125432 (2016).
[17]S. Sullivan, A. Vallabhaneni, I. Kholmanov, X. Ruan, J. Murthy, and L. Shi, Nano Lett. **17**, 2049 (2017).
[18]T. Feng, W. Yao, Z. Wang, J. Shi, C. Li, B. Cao, and X. Ruan, Phys. Rev. B **95**, 195202 (2017).
[19]M. An, Q. Song, X. Yu, H. Meng, D. Ma, R. Li, Z. Jin, B. Huang, and N. Yang, Nano Lett. **17**, 5805 (2017).
[20]A. Majumdar and P. Reddy, Appl. Phys. Lett. **84**, 4768 (2004).
[21]Y. Wang, X. Ruan, and A. K. Roy, Phys. Rev. B **85**, 205311 (2012).
[22]Z. Li, S. Tan, E. Bozorg-Grayeli, T. Kodama, M. Asheghi, G. Delgado, M. Panzer, A. Pokrovsky, D. Wack, and K. E. Goodson, Nano Lett. **12**, 3121 (2012).
[23]X. Wu and T. Luo, EPL **110**, 67004 (2015).
[24]Z. Lu, Y. Wang, and X. Ruan, J. Appl. Phys. **123**, 074302 (2018).
[25]J. Shi, X. Yang, T. S. Fisher, and X. Ruan, e-print arXiv:1812.07910 (2018).
[26]P. E. Hopkins and P. M. Norris, Appl. Surf. Sci. **253**, 6289 (2007).
[27]P. E. Hopkins, J. L. Kassebaum, and P. M. Norris, J. Appl. Phys. **105**, 023710 (2009).
[28]Z. Lu, Y. Wang, and X. Ruan, Phys. Rev. B **93**, 064302 (2016).
[29]D. Singh, J. Murthy, and T. Fisher, in *ASME 2009 InterPACK Conference* (ASME, 2009), Vol. 1, pp. 575–591.
[30]Z. Lu, A. Vallabhaneni, B. Cao, and X. Ruan, Phys. Rev. B **98**, 134309 (2018).
[31]D. Singh, J. Y. Murthy, and T. S. Fisher, J. Appl. Phys. **110**, 094312 (2011).
[32]D. Singh, J. Y. Murthy, and T. S. Fisher, J. Appl. Phys. **110**, 044317 (2011).
[33]T. Zeng and G. Chen, Microscale Thermophys. Eng. **5**, 71 (2001).